

MIT Open Access Articles

*Nickel-Borate Oxygen-Evolving Catalyst
that Functions under Benign Conditions*

The MIT Faculty has made this article openly available. **Please share**
how this access benefits you. Your story matters.

Citation: Dinca, Mircea, Yogesh Surendranath, and Daniel G. Nocera. "Nickel-borate oxygen-evolving catalyst that functions under benign conditions." PNAS June 8, 2010 vol. 107 no. 23 10337-10341 ©2010 by the National Academy of Sciences.

As Published: <http://dx.doi.org/10.1073/pnas.1001859107>

Publisher: National Academy of Sciences

Persistent URL: <http://hdl.handle.net/1721.1/61393>

Version: Final published version: final published article, as it appeared in a journal, conference proceedings, or other formally published context

Terms of Use: Article is made available in accordance with the publisher's policy and may be subject to US copyright law. Please refer to the publisher's site for terms of use.



Nickel-borate oxygen-evolving catalyst that functions under benign conditions

Mircea Dincă, Yogesh Surendranath, and Daniel G. Nocera¹

Department of Chemistry, Massachusetts Institute of Technology, 77 Massachusetts Avenue, Cambridge, MA 02139-4307

This contribution is part of the special series of Inaugural Articles by members of the National Academy of Sciences elected in 2009.

Contributed by Daniel George Nocera, April 8, 2010 (sent for review December 26, 2009)

Thin catalyst films with electrocatalytic water oxidation properties similar to those of a recently reported Co-based catalyst can be electrodeposited from dilute Ni²⁺ solutions in borate electrolyte at pH 9.2 (B_i). The Ni-B_i films can be prepared with precise thickness control and operate at modest overpotential providing an alternative to the Co catalyst for applications in solar energy conversion.

artificial photosynthesis | nonlegacy | personalized energy | water splitting | energy storage

Global energy need will roughly double by midcentury and triple by 2100. Most of that demand is driven by 3 billion low-energy users in the nonlegacy world and by 3 billion people yet to inhabit the planet over the next half century (1). Research targets that meet the energy need of these 6 billion new energy users provide global society with a direct path to providing a solution for a sustainable and carbon-neutral energy future. Moreover, because energy use scales with wealth (2), geopolitical and economic stability is greatly enhanced by abundant and clean energy as it enables individuals in the smallest village in the nonlegacy world and in the largest city of the legacy world to coexist more equitably. However, the task of supplying energy to the nonlegacy world will not be an easy one. To achieve the target of a carbon-neutral energy supply for the nonlegacy world will require the delivery of energy on a scale commensurate with, or larger than, the entire present-day energy supply from all sources combined (3).

The success in meeting the energy challenge in the nonlegacy world will largely depend on the design, research, and development of new technologies that are at odds with energy systems of the legacy world. Energy systems of the past and present operate at large scale, they are centralized, and energy is distributed to the masses. Such infrastructure is not compatible to the near-term needs of the nonlegacy world where it is cost prohibitive to build centralized energy and distribution systems. An alternative strategy that is better adapted to making energy available to the 6 billion new energy users is highly distributed energy systems for the individual—a personalized energy (PE) (4, 5)—that places a premium on low cost, even if efficiency must be sacrificed up front.

Low cost in a manufacturing environment is most profoundly affected by materials goods of the system (most generalized by the weight of the system) and the production volume (6, 7). Here again, the nonlegacy and legacy worlds diverge. Large, centralized, and efficient energy systems come with significant balance-of-system (BOS) costs. Down-scaling such technology does not scale economically because the BOS costs do not scale commensurately. Thus, off-the-shelf technologies will be difficult to adapt to low-cost energy systems. Rather, the disruptive energy technologies of the future will be those that conform to the message of *lightweight* and *high-volume manufacturing*. Simply put, new research and development are needed to provide the nonlegacy world with the “fast food” equivalent of energy systems.

Solar PE is particularly well adapted to meeting the energy needs of the nonlegacy world. It is highly distributed and available to all. And low-cost and large-scale manufacturing are already an

emerging trend in the deployment of photovoltaics (8). However, low-cost photovoltaics are not enough. Because local insolation is diurnal, solar energy cannot be used as a large-scale energy supply unless it can be stored. Most current methods of solar storage are characterized by low-energy densities and consequently they present formidable challenges for large-scale solar implementation. This includes batteries, which have low-energy density (0.5 MJ/kg with a ceiling of ~3.0 MJ/kg). Conversely, the energy density of fuels is $\geq 10^2$ larger and H₂ is $\geq 10^3$ larger than the upper limit of battery storage capacity. Indeed, society has intuitively understood this disparity in energy density as all large-scale energy storage is in the form of fuels. But these fuels are carbon based. An imperative for our research has been to develop fuel storage methods that are carbon-neutral, sustainable, easily scalable, and inexpensive.

We have taken important steps towards meeting this imperative by developing a cobalt oxygen-evolving catalyst (Co-OEC) (9, 10) that can use an energy input from a photoanode or photovoltaic to split water into hydrogen and oxygen. Co-OEC is unique because it (i) is a functional model of the oxygen-evolving complex of Photosystem II (11), (ii) operates safely with high activity under benign conditions (room temperature and pH 7) (9, 10), (iii) is comprised of inexpensive, Earth-abundant materials and is easy to manufacture (9, 10), (iv) is self-healing (12), (v) is functional in natural, waste, and salt water (10, 11), (vi) can form on diverse conducting surfaces of varying geometry and be easily interfaced with a variety of light-absorbing and charge-separating materials (11), and (vii) may be activated by solar-derived electricity or directly by sunlight mediated by a semiconductor (13, 14). The simple operation of the catalyst from impure water sets a path to providing distributed solar and clean drinking water (5).

We now report that thin catalyst films with O₂ evolution properties can be electrodeposited from dilute Ni²⁺ solutions in borate electrolyte at pH 9.2 (B_i). The Ni-B_i films can be prepared with precise thickness control and operate at modest overpotential providing an alternative to the Co-OEC catalyst for applications in solar energy storage and water purification.

Results

Fig. 1 shows the onset of a catalytic wave at 1.2 V [vs. normal hydrogen electrode (NHE)] on the first anodic sweep of a glassy carbon electrode immersed in a 0.1 M H₂BO₃/H₃BO₃ electrolyte (B_i electrolyte) solution at pH 9.2 containing 1 mM of Ni²⁺ ion. The cathodic return scan exhibits a broad feature at $E_{p,c} = 0.87$ V, attributed to the reduction of a surface adsorbed species formed during the initial sweep through the catalytic wave. Subsequent cyclic voltammetry (CV) scans display a sharp

Author contributions: D.G.N. designed research; M.D. and Y.S. performed research; and M.D., Y.S., and D.G.N. wrote the paper.

The authors declare no conflict of interest.

¹To whom correspondence should be addressed. E-mail: nocera@mit.edu.

This article contains supporting information online at www.pnas.org/lookup/suppl/doi:10.1073/pnas.1001859107/-DCSupplemental.

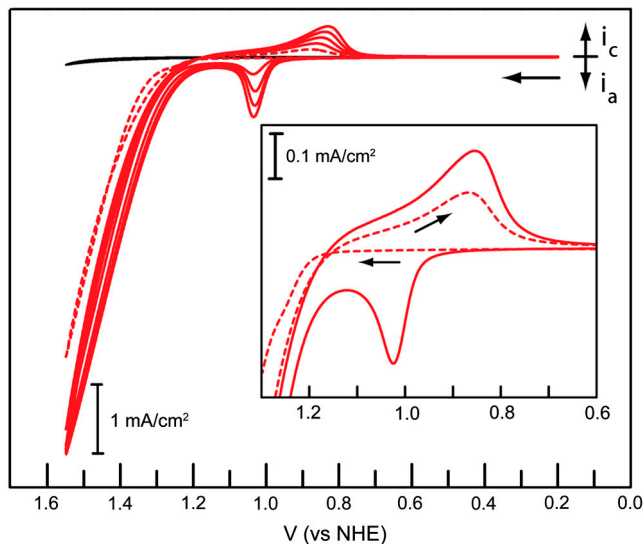


Fig. 1. CVs using a glassy carbon working electrode, 50 mV/s scan rate, of aqueous 1 mM Ni^{2+} in 0.1 M B_i electrolyte, pH 9.2. Successive scans show an increase of the anodic peak current for the redox event centered at ~ 1.0 e. (Inset) First (---) and second (—) CV scans using a glassy carbon working electrode, 50 mV/s scan rate, of aqueous 1 mM Ni^{2+} solutions in 0.1 M B_i electrolyte, pH 9.2. CV trace in the absence of Ni^{2+} is shown as a black trace.

anodic prefeature centered at $E_{p,a} = 1.02$ V and a cathodically shifted catalytic wave with an onset potential of 1.15 V. As shown in Fig. 1, the anodic and the cathodic prefeatures increase in amplitude with scanning, suggesting the growth of a surface-deposited material. By integration of the anodic prefeature, we estimate that a monolayer of catalyst is deposited after a single CV scan at 50 mV/s, whereas a film of 10–12 layers thick is produced after 20 scans, thus attesting to the controlled nature of the electrodeposition. Neither film formation nor catalysis is observed in the absence of the B_i electrolyte. Indeed, a CV of a 1 mM aqueous solution of Ni^{2+} in 0.1 M NaNO_3 electrolyte at pH 9.2 is indistinguishable from the electrode background in the absence of Ni^{2+} (Fig. S1). As was the case with Co-OEC (10), this suggests that a proton-accepting electrolyte, such as borate, is essential for facile electrodeposition and catalysis.

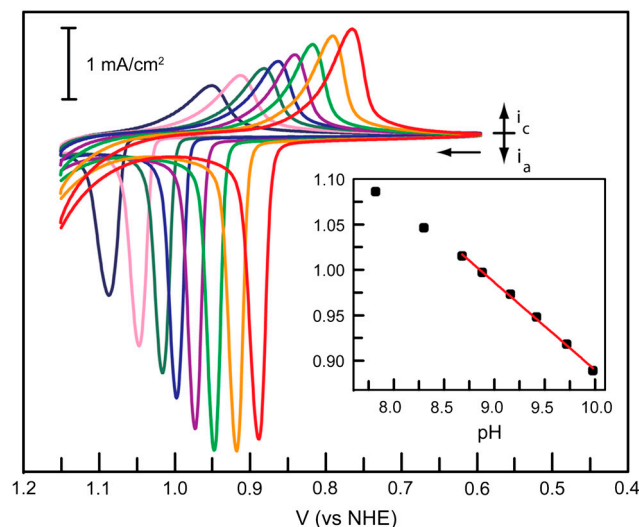


Fig. 2. CVs scans of a Ni borate catalyst film at pH values of 7.82, 8.30, 8.68, 8.88, 9.16, 9.42, 9.72, and 9.98 in. going from left to right, respectively. The inset shows a linear fit for the 8.7–10.0 pH region, with a slope of 96 mV/pH unit. The CVs were taken at scan rates of 50 mV/s.

The CV features observed for the Ni- B_i system are similar to those observed of Ni oxide thin films (15–22). For instance, electrodeposited $\text{Ni}(\text{OH})_2$ films display an anodic prefeature centered at ~ 0.65 – 1.25 V, depending on pH, which is typically assigned to a $1e^- - 1H^+$ redox couple, $\text{Ni}^{\text{II}}(\text{OH})_2/\text{Ni}^{\text{III}}\text{O}(\text{OH})$ (23–26). To examine if proton-coupled electron transfer is operational in our system, (27, 28) we measured the pH dependence of the anodic prefeature (see Fig. 2). Surprisingly, CV experiments conducted at a scan rate of 50 mV/s give rise to a plot of $E_{p,a}$ vs. pH with a slope of -96 mV/pH unit. Similar slopes, -91 and -89 mV/pH unit, were obtained at scan rates of 10 and 5 mV/s, respectively (Fig. S2). These values are much higher than the theoretical value of -59 mV expected for the $1e^- - 1H^+$ oxidation of $\text{Ni}^{\text{II}}(\text{OH})_2$ to $\text{Ni}^{\text{III}}\text{O}(\text{OH})$. Rather, a slope of -90 mV/pH unit corresponds to the loss of $1e^-$ accompanied by the transfer of ~ 1.5 protons. This suggests that a $2e^- - 3H^+$ couple may be operative, as has been proposed for the dimerization of Ir^{IV} hydro-hydroxo species to form iridium oxide: $2[\text{IrO}_2(\text{OH})_2]^{2-} + 2e^- + 3\text{H}_2\text{O} \leftrightarrow [\text{Ir}_2\text{O}_3(\text{OH})_3 \cdot 2\text{H}_2\text{O}]^{3-} + 3\text{OH}^-$ (29, 30), which exhibits an observed slope of -88 mV/pH unit.

To further probe the morphology, composition, and structure of the electrodeposited material, thicker films of Ni- B_i were electrodeposited onto indium-tin oxide (ITO) covered glass slides by subjecting 1 mM Ni^{2+} solutions in B_i electrolyte to bulk electrolysis at 1.3 V. During electrodeposition, the current density rapidly attains a plateau value of ~ 1.4 mA/cm², as shown in Fig. 3. A 3–4- μm -thick film is grown by passing 10 C/cm² at 1.3 V. Scanning electron microscopy and powder X-ray diffraction of this film reveal that it is relatively smooth and amorphous (see Fig. 3 Inset and Figs. S3 and S4, respectively). To interrogate the catalyst composition, thick films were grown on large surface area electrodes, and then dried in the air. Elemental analysis of the dried material revealed a formula of $\text{Ni}^{\text{III}}\text{O}(\text{OH})_{2/3}(\text{H}_2\text{BO}_3)_{1/3} \cdot 1.5\text{H}_2\text{O}$, which we understand may differ from that of the catalyst under wet and operational conditions. Nevertheless, the formula of Ni- B_i is reminiscent of $\text{NiO}(\text{OH})$, which exhibits O_2 evolution under similar pH conditions and is an effective water oxidation catalyst in concentrated alkali solution (24).

The potential-dependent O_2 evolution activity of Ni- B_i , evaluated in Ni^{2+} -free B_i electrolyte at pH 9.2, is in line with that observed for $\text{NiO}(\text{OH})$ under highly alkaline conditions. Faradaic efficiency for O_2 evolution, as measured by fluorescence detec-

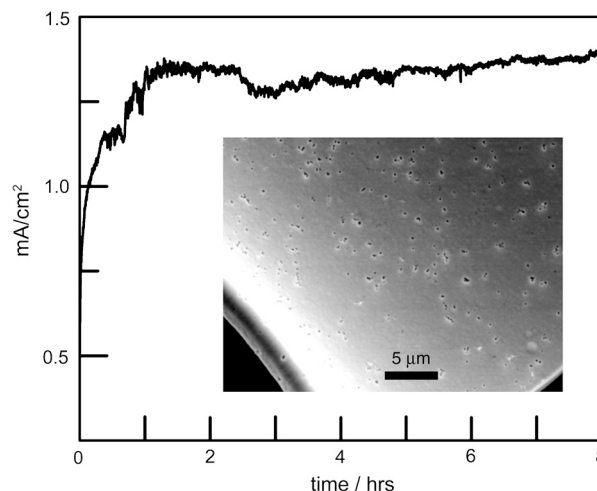


Fig. 3. Current density trace for bulk electrolysis at 1.30 V in 0.1 M B_i electrolyte, pH 9.2, 1 mM Ni^{2+} using an ITO anode. Irregularities are due to bubble formation and to stirring. The inset shows an SEM photograph of a film obtained by passing 10 C/cm² at 1.30 V.

tion, is quantitative (Fig. S5). The current density for O_2 evolution, j , obtained for a thin film grown by passing 300 mC/cm^2 was measured as a function of the overpotential, η . A plot of $\log(j)$ vs. η (Tafel plot, Fig. 4) produces a slope of $\sim 59 \text{ mV/decade}$ for current densities ranging from 1 mA/cm^2 to $7 \mu\text{A/cm}^2$. Notably, preconditioning the electrode by subjecting it to 12 h of preelectrolysis at a current density of $\sim 1 \text{ mA/cm}^2$ is necessary to obtain reproducible values of the Tafel slope. Indeed, measurements performed on fresh Ni-B_i films without preconditioning produced Tafel slopes of up to 120 mV/decade , outside the range of $40\text{--}80 \text{ mV/decade}$ reported for typical Ni oxides (31, 32).

Very thin films of Ni-B_i are stable to cathodic bias, as demonstrated by cycling an electrodeposited film through 100 CV scans with a switching potential below the catalytic wave (1.1 V). Catalysis was still operative after these cycles, and the peak current of the anodic prefeature drops by only $\sim 16\%$ during the cycling experiment (Fig. S6). The stability of the Ni-B_i film to a cathodic bias on the CV timescale suggests that this material may also exhibit activity for O_2 reduction, a possibility that is being explored currently.

In summary, a Ni-based oxide catalyst can be deposited in a highly controllable fashion under mild conditions from dilute Ni^{2+} solutions in the presence of borate. Deposition routes mimicking those employed for the formation of a related Co OEC give rise to a Ni-based catalyst that evolves O_2 in near-neutral conditions with an activity of 1 mA/cm^2 at an overpotential of $\sim 425 \text{ mV}$. The catalyst exhibits long-term stability in water with no observed corrosion. The results reported here contribute to an expanding group of water splitting catalysts that operate under mild conditions and at current densities commensurate with non-concentrated solar photovoltaic outputs ($5\text{--}20 \text{ mA/cm}^2$). The simple operating conditions may permit energy storage to be performed with devices that are inexpensive and highly manufacturable.

Experimental Methods

Materials. $Ni(NO_3)_2 \cdot 6H_2O$ 99.9985% was used as received from Strem. H_3BO_3 99.5%, $NaNO_3$, and KOH 85% were used as received from Sigma-Aldrich. $NaOH$ 99% was used as received from Mallinckrodt. All buffers were prepared with reagent-grade water (Ricca Chemical, $18 \text{ M}\Omega\text{-cm}$ resistivity). ITO-coated glass slides ($8\text{--}12 \Omega/\text{sq}$ surface resistivity) and fluorine-tin-oxide

(FTO) coated glass slides were purchased from Sigma-Aldrich and from Hartford Glass, respectively.

Electrochemical Methods. All electrochemical experiments were performed at ambient temperature in air-saturated solutions with a CH Instruments 760C potentiostat and a BASi Ag/AgCl reference electrode. All electrode potentials were converted to the NHE scale using $E(\text{NHE}) = E(\text{Ag/AgCl}) + 0.197 \text{ V}$. Unless otherwise stated, the electrolyte was 0.1 M potassium borate at pH 9.2 (B_i electrolyte).

Cyclic Voltammetry. A 0.07 cm^2 glassy carbon button electrode was used as the working electrode and Pt wire as the auxiliary electrode. The working electrode was polished with 0.3 and $0.05 \mu\text{m}$ alumina particles for 30 s each and thoroughly rinsed with reagent-grade water prior to use. Unless otherwise noted, cyclic voltammograms (CVs) were collected with compensated cell resistance (iR) at 50 mV/s and 0.01 or 0.1 mA/V sensitivity in Ni-free B_i electrolyte, and B_i electrolytes containing $1 \text{ mM } Ni^{2+}$.

To determine the surface catalyst coverage on a glassy carbon electrode, the integrated charge of the anodic prefeature was taken as a direct estimate of the number of Ni atoms electrodeposited. Monolayer coverage was approximated as a surface density of $5 \text{ Ni atoms}/25 \text{ \AA}^2$ implying that an integrated charge of $\sim 300 \mu\text{C/cm}^2$ corresponds to one monolayer of catalyst.

To verify the necessity of using an electrolyte with good proton-accepting ability, a CV was taken with a glassy carbon electrode of a $0.1 \text{ M } NaNO_3$ solution whose pH was adjusted to 9.2 using concentrated KOH . Upon addition of $1 \text{ mM } Ni^{2+}$ to this solution, the CV trace was identical to that of the background, indicating that the presence of a proton-accepting electrolyte (such as borate) is essential for catalyst formation and activity (Fig. S1).

To determine the dependence of the anodic prefeature with pH, a catalyst film was prepared on a 0.07 cm^2 glassy carbon electrode by running 13–15 consecutive CV cycles in a $1 \text{ mM } Ni^{2+}/0.1 \text{ M B}_i$ solution with a switching potential of 1.4 V . The working electrode was then thoroughly rinsed with reagent-grade water and placed in a fresh Ni-free B_i solution of 0.1 M . This solution had an initial pH of 7.82. The pH was gradually increased by adding small aliquots of KOH solution, and CVs were recorded at each pH point with a scan rate of 50 mV/s . CVs at all pH points were taken with iR compensation using solution resistance values measured prior to each CV.

To verify the stability of a thin catalyst film, a polished electrode was used to record a CV in $1 \text{ mM } Ni^{2+}$ solution with a switching potential of 1.5 V . After the first full scan, the electrode was removed, rinsed with reagent-grade water, and placed into a Ni-free B_i solution. One hundred consecutive CV scans were recorded with a switching potential of 1.1 V . An insignificant decrease in current density was observed for the anodic prefeature centered at $\sim 1 \text{ V}$ (Fig. S6). To verify that a competent catalyst was still present on the electrode after this treatment, the same electrode was cycled past the onset potential ($>1.1 \text{ V}$); a large catalytic wave was observed, attesting that the catalyst film is stable to reductive bias on the CV timescale.

Bulk Electrolysis and in Situ Catalyst Formation. Bulk electrolyses were performed in a two-compartment electrochemical cell with a glass frit junction of fine porosity. For catalyst electrodeposition, the auxiliary compartment was charged with $\sim 40 \text{ mL}$ of 0.1 M B_i electrolyte and the working compartment was charged with 40 mL of solution obtained by combining 20 mL of 0.2 M B_i electrolyte and 20 mL of $2 \text{ mM } Ni^{2+}$ solution. The B_i electrolyte solution became turbid immediately following the addition of Ni^{2+} solution [likely due to the formation of $Ni(OH)_2$]. The solution was filtered through a $0.45 \mu\text{m}$ filter (Pall Acrodisc) prior to electrolysis. The filtered Ni-B_i solution remained clear for several hours and during the entire duration of electrodeposition experi-

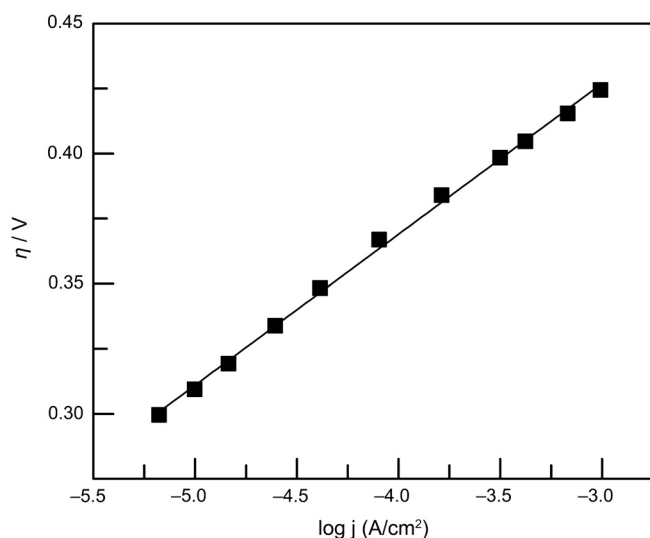


Fig. 4. Tafel plot, $\eta = (V_{\text{appl}} - iR - E^0)$, of a Ni-B_i catalyst film operated in 0.2 M B_i , pH 9.2 where η is the overpotential, iR accounts for the uncompensated solution resistance, and E^0 is the thermodynamic potential for water oxidation at this pH (0.69 V vs. NHE). The slope of the line is 58 mV/decade .

ments. The working electrode was a 1×2.5 cm piece of ITO-coated glass cut from a commercially available slide. Typically, a 1 cm^2 area of the electrode was exposed to the solution. Pt mesh was used as the auxiliary electrode. Electrolysis was carried out at 1.30 V with stirring and without iR compensation and with the reference electrode placed 2–3 mm from the ITO surface.

Tafel Plot Data Collection. Current-potential data were obtained by performing controlled potential electrolyses in B_i electrolytes at a variety of applied potentials in two-compartment cells containing ~ 40 mL of fresh electrolyte on each side. Prior to data collection, the solution resistance was measured with a clean ITO working electrode using the iR test function. The working ITO electrode and the Ag/AgCl reference electrode were kept in the same configuration while the electrolysis cell was replaced with one containing Ni^{2+} in the working compartment, as described above. A 1 cm^2 catalyst film was prepared via an electrodeposition that passed 300 mC/cm^2 . Working and reference electrodes were subsequently rinsed in reagent-grade water and all electrodes were reimmersed in a two-compartment electrochemical cell containing fresh B_i electrolyte in both compartments. A current of $950 \mu\text{A/cm}^2$ was applied for ~ 12 h prior to collecting data for the Tafel plot. Steady-state currents were measured at a variety of applied potentials while the solution was stirred, proceeding in 10–25 mV steps between 1.15 and 0.99 V. Typically, the current reached a steady-state at a particular potential in 2–5 min and current values were read after 7–10 min. Measurements were made twice. The variation in steady-state current between two runs at a particular potential was $<5\%$. The solution resistance measured prior to the data collection (36Ω) was used to correct the Tafel plot for iR drop (Fig. 4).

Elemental Analyses. Microanalyses were performed by Columbia Analytics. The Ni-Bi catalyst was prepared on large surface area ($\sim 25 \times 25$ cm) FTO-coated glass slides using filtered $1 \text{ mM Ni}^{2+}/0.1 \text{ M Bi}$ solutions. Upon termination of the electrolyses, the slides were immediately removed from the solution, rinsed with reagent-grade water, and allowed to dry in air. The electrodeposited material was carefully scraped off using a razor blade and the material was submitted for microanalysis. The elemental composition for a sample prepared as above was as follows: Ni, 43.6 wt. %; H, 2.16 wt. %; B, 2.7 wt. %; and K, 1.1 wt. %. Although an idealized catalyst formula of $\text{Ni}^{\text{III}}\text{O}(\text{OH})_{2/3}(\text{H}_2\text{BO}_3)_{1/3} \cdot 1.5\text{H}_2\text{O}$ matches these values, it is unlikely that the composition of a dry film corresponds exactly to that of a film under operational conditions.

Scanning Electron Microscopy. SEM micrographs were obtained with a JSM-5910 microscope (JEOL). Following electrodeposition, catalyst samples were rinsed with deionized water and allowed to dry in air before loading into the instrument. Images were obtained with an acceleration voltage of 5–10 kV. Fig. S3 displays SEM images of a catalyst prepared by passing 10 C/cm^2 at 1.3 V.

Powder X-Ray Diffraction. A powder X-ray diffraction pattern for a film grown by passing 10 C/cm^2 was obtained with a Rigaku RU300 rotating anode X-ray diffractometer (185 mm) using

Cu $K\alpha$ radiation ($\lambda = 1.5405 \text{ \AA}$). As shown in Fig. S4, the only peaks in the diffraction pattern correspond to those pertaining to the ITO background, indicating that the electrodeposited nickel oxide catalyst is amorphous.

Spectroelectrochemistry. Spectra were recorded on a Spectral Instruments 400 series diode array spectrometer. The working electrode consisted of a 2×0.8 cm piece of ITO-coated quartz cut from a commercially available slide (Delta Technologies, Inc.). Working, reference, and Pt auxiliary electrodes were fitted into a standard 1-cm path-length UV-Vis cuvette to comprise a one compartment electrolysis cell. The spectrometer was blanked against a filtered solution of B_i electrolyte containing Ni^{2+} (1 mM) and spectra were collected periodically while 1.2 V was applied. The spectrum recorded after 9 min of electrolysis is shown in Fig. S7.

Determination of Faradaic Efficiency. An Ocean Optics oxygen sensor system was used to detect O_2 quantitatively. The experiment was performed in a custom-built two-compartment gas-tight electrochemical cell with a 14/20 port on each compartment and a Schlenk connection with a Teflon valve on the working compartment. The B_i electrolyte was degassed by bubbling with high purity N_2 for 12 h with vigorous stirring, and it was transferred to the electrochemical cell under N_2 . One compartment contained a Ni foam auxiliary electrode and the other compartment contained the working and Ag/AgCl reference electrodes. The Ni catalyst was prepared from an electrodeposition as described above. The reference electrode was positioned several millimeters from the surface of the catalyst. The 14/20 port of the working compartment was fitted with a FOXY OR125–73 mm O_2 sensing probe connected to a MultiFrequency Phase Fluorometer. The phase shift of the O_2 sensor on the FOXY probe, recorded at 10 s intervals, was converted into the partial pressure of O_2 in the headspace using a two-point calibration curve (air, 20.9% O_2 , and high purity N_2 , 0% O_2). After recording the partial pressure of O_2 for 1 h in the absence of an applied potential, electrolysis was initiated at 1.3 V without iR compensation.

For determination of Faradic efficiency in the B_i buffer, electrolysis with O_2 sensing was continued until 53.5 C passed. Upon terminating the electrolysis, the O_2 signal reached a plateau over the course of the next 3 h. During this time, the O_2 level had risen from 0% to 6.98%. At the conclusion of the experiment, the volume of the solution (59.5 mL) and the volume of the headspace (48.0 mL) in the working compartment were measured. The total charge passed in the electrolysis was divided by 4 F to get a theoretical O_2 yield of $138.3 \mu\text{mol}$. The measured partial pressure of O_2 was corrected for dissolved O_2 in solution using Henry's Law and converted, using the ideal gas law, into a measured O_2 yield of $143.4 \mu\text{mol}$ ($103.7\% \pm 5\%$) (Fig. S5).

ACKNOWLEDGMENTS. This work was supported by a National Science Foundation (NSF) Center for Chemical Innovation (CCI Powering the Planet, Grants CHE-0802907 and CHE-0947829), Air Force Office of Scientific Research FA9550-09-1-0689, and a grant from The Chesonis Family Foundation. Y.S. gratefully acknowledges the NSF Graduate Research Fellowship Program for a predoctoral fellowship.

- Lewis NS, Nocera DG (2006) Powering the planet: Chemical challenges in solar energy utilization. *Proc Natl Acad Sci USA* 103:15729–15735.
- Hoffert MJ, et al. (1998) Energy implications of future stabilization of atmospheric CO_2 content. *Nature* 395:881–884.
- Nocera DG (2006) On the future of global energy. *Daedalus* 135:112–115.
- Nocera DG (2009) Personalized energy: The home as a solar power station and solar gas station. *ChemSusChem* 2:387–390.
- Nocera DG (2009) Chemistry of personalized solar energy. *Inorg Chem* 48:10001–10007.
- Malstrom EM (1981) *What Every Engineer Should Know About Manufacturing Cost Estimating* (Dekker, New York), Chap. 2.
- Swamidass PM (2000) *Encyclopedia of Production and Manufacturing Management* (Kluwer, Boston).
- Ginley D, Green MA, Collins R (2008) Solar energy conversion toward 1 terawatt. *MRS Bull* 33:355–364.
- Kanan MW, Nocera DG (2008) In situ formation of an oxygen-evolving catalyst in neutral water containing phosphate and Co^{2+} . *Science* 321:1072–1075.
- Surendranath Y, Dincă M, Nocera DG (2009) Electrolyte-dependent electrosynthesis and activity of cobalt based water oxidation catalysts. *J Am Chem Soc* 131:2615–2620.
- Kanan MW, Surendranath Y, Nocera DG (2009) Cobalt-phosphate oxygen-evolving compound. *Chem Soc Rev* 38:109–114.

12. Lutterman DA, Surendranath Y, Nocera DG (2009) A self-healing oxygen-evolving catalyst. *J Am Chem Soc* 131:3838–3839.
13. Zhong DK, Sun J, Inumaru H, Gamelin DR (2009) Solar water oxidation by composite catalyst/ α -Fe₂O₃ photoanodes. *J Am Chem Soc* 131:6086–6087.
14. Steinmiller EMP, Choi KS (2009) Photochemical deposition of cobalt-based oxygen evolving catalyst on a semiconductor photoanode for solar oxygen production. *Proc Natl Acad Sci USA* 106:20633–20636.
15. Macdougall B, Graham MJ (1981) Growth of thick anodic oxide-films on nickel in borate buffer solution. *J Electrochem Soc* 128:2321–2325.
16. Gassa LM, Vilche JR, Arvia AJ (1983) A potentiodynamic study of anodic film formation on nickel in borate solutions. *J Appl Electrochem* 13:135–145.
17. Abd El, Aal EE (2003) Anodic oxide films on nickel electrode in borate solutions. *Corros Sci* 45:641–658.
18. Tench D, Warren LF (1983) Electrodeposition of conducting transition-metal oxide hydroxide films from aqueous-solution. *J Electrochem Soc* 130:869–872.
19. Chen YWD, Noufi RN (1984) Electrodeposition of nickel and cobalt oxides onto platinum and graphite-electrodes for alkaline water electrolysis. *J Electrochem Soc* 131:1447–1451.
20. Morisaki S, Kawakami K, Baba N (1988) Formation of nickel oxyhydroxide thin-films by electrodeposition and their electrochromic characteristics. *Jpn J Appl Phys* 27:314–318.
21. Chigane M, Ishikawa M (1992) Characterization of electrochromic nickel-oxide thin-films prepared by anodic deposition. *J Chem Soc Faraday T* 88:2203–2205.
22. Chigane M, Ishikawa M, Inoue H (2000) Further XRD characterization of electrochromic nickel oxide thin films prepared by anodic deposition. *Sol Energy Mat Sol C* 64:65–72.
23. Oliva P, et al. (1982) Review of the structure and the electrochemistry of nickel hydroxides and oxy-hydroxides. *J Power Sources* 8:229–255.
24. Corrigan DA, Bendert RM (1989) Effect of coprecipitated metal-ions on the electrochemistry of nickel-hydroxide thin-films—cyclic voltammetry in 1 M KOH. *J Electrochem Soc* 136:723–728.
25. Lyons MEG, Brandon MP (2008) The oxygen evolution reaction on passive oxide covered transition metal electrodes in aqueous alkaline solution. Part 1—nickel. *Int J Electrochem Sci* 3:1386–1424.
26. Wruck DA, Rubin M (1993) Structure and electronic-properties of electrochromic NiO films. *J Electrochem Soc* 140:1097–1104.
27. Cukier RI, Nocera DG (1998) Proton-coupled electron transfer. *Annu Rev Phys Chem* 49:337–369.
28. Reece SY, Nocera DG (2009) Proton-coupled electron transfer in biology: Results from synergistic studies in natural and model systems. *Annu Rev Biochem* 78:673–699.
29. Burke LD, Whelan DP (1984) A voltammetric investigation of the charge storage reactions of hydrous iridium oxide layers. *J Electroanal Chem* 162:121–141.
30. Burke LD, Whelan DP (1981) A new interpretation of the charge storage and electrical-conductivity behavior of hydrous iridium oxide. *J Electroanal Chem* 124:333–337.
31. de Chialvo MRG, Chialvo AC (1988) Oxygen evolution reaction on thick hydrous nickel-oxide electrodes. *Electrochim Acta* 33:825–830.
32. Wang XY, Luo H, Yang HP, Sebastian PJ, Gamboa SA (2004) Oxygen catalytic evolution reaction on nickel hydroxide electrode modified by electroless cobalt coating. *Int J Hydrogen Energy* 29:967–972.